Available online at www.sciencedirect.com
ScienceDirect
Journal of Catalysis 255 (2008) 79–93
JOURNAL OF CATALYSIS
www.elsevier.com/locate/jcat

Role of Pt on PtGaZr/SiO_2 catalyst in light naphtha isomerization

Roberto Galiasso Tailleur [*,1], Jose Bonilla Platin

Department of Thermodynamics, Simon Bolivar University, Sartenejas, Caracas, Venezuela

Received 25 August 2007; revised 9 January 2008; accepted 11 January 2008

Abstract

The effect of Pt content on the light naphtha isomerization reaction was studied using PtGaZr/SiO_2-type catalysts. The catalysts were characterized by XPS, IR, pyridine, and CO adsorption, and by chemical reaction. The reaction was studied in a radial plug flow-type gas-phase reactor at three temperature levels, residence times, and hydrogen partial pressures. Other exploratory tests involved adding 20% of 1-pentene, cyclopentane, or isopentane to the feedstock. The results indicate that Pt is incorporated into the Ga–Zr and Ga–Si cluster, which is generated by migration of Ga and Zr to the surface of the silica. The Pt slightly modifies the number, activity, and selectivity of the acid sites, but its most important role is on catalyst stability. It was found that some $Pt^{\delta+}$ species may be located in the border of the crystal, and Pt^{2+} species may be found in the subsurface of the clusters. A mechanism of two isomerization acid sites proposed, and an apparent kinetics model for light naphtha isomerization is used to predict the isomer yields in a gas-phase radial reactor. The role of catalysts surface composition in chemical reactions is discussed.

Keywords: Light naphtha isomerization; Platinum; PtGaZr/SiO_2; Radial reactor; Mechanism of reaction

1. Introduction

N-pentane is an important component in the refining and petrochemical industry; in particular, there is a strong demand [1] for the isoparaffinic C_5–C_6 cut with a high octane number. The light naphthas comply with environmental regulations for clean fuels and thus are good candidates to complement the alkylate component in the gasoline pool. Active and stable catalysts require the presence of a noble metal (generally platinum) as well as hydrogen to prevent catalyst deactivation [2,3].

There is a vast array of literature on butane isomerization (using mainly platinum on sulfated zirconium catalysts), where different influences of hydrogen partial pressures on the rate of the isomerization are reported (going from a positive to a negative [4] order of reaction). In commercial practice with pentanes and hexanes, isomerization on a Pt/zeolite catalyst is done at lower temperatures (450–500 K) than required for butane isomerization. Typical catalysts containing 0.5 wt% Pt show a positive reaction rate [4] with respect to hydrogen. Most authors have noted that hydrogen activated on platinum is a source of protons and hydride species. The presence of a hydrogen excess seems to inhibit the reaction by competing with the intermediate compounds for the active sites, but preserves the catalyst stability. Watanabe et al. [5] demonstrated that the Pt–SO_4ZrO_2 (PtSZr) catalyst is more active, selective, and stable for the isomerization of light naphtha than SO_4ZrO_2 (SZr). Testing PtSO_4ZrO_2–Al_2O_3 (PtSZrAl), they observed high initial activity but also significant deactivation. From the other side, the Ga/FMI and PtGa/FMI catalysts have been extensively studied for the oligomerization of short paraffin and olefins to aromatics ([6–8], among others).

In previously unpublished results, we found a positive effect of hydrogen partial pressure on PtGaZr/SiO_2 and PtGa/SiO_2 catalysts with Pt loadings of 0.3–0.6% when using 1-pentene as feed [9]. Other PtGaZr/SiO_2 catalysts with higher Ga and Zr contents on siliceous MCM-41-type structures also were used to produce cyclohexane and isoparaffin from ethylene and propylene [10]. Recently, a new PtGaZr/SiO_2 (PtGaZr) catalyst was developed in which Pt may be located in a different structure than in the conventional PtGa$_2$O$_3$/SiO_2 (PtGa)

* Corresponding author.
E-mail address: galiassa@cantv.net (R.G. Tailleur).
[1] Present address: Department of Chemical Engineering, TA&M University, College Station, TX 77843, USA.

0021-9517/$ – see front matter
doi:10.1016/j.jcat.2008.01.010

or $PtZrO_2/SiO_2$ (PtZr) zeolites. In the present study, we concentrated on the analysis of the effect of Pt on the new catalyst for the isomerization of light naphtha—a pentane-rich stream—obtained from the refinery. To interpret the activity and selectivity results, we used a two-active-sites model and characterized the catalyst to determine the effect of Pt on these sites.

2. Experimental

2.1. Catalyst preparation

The catalysts were prepared in a Teflon-lined autoclave using a modification of the method of Wu et al. [11], who synthesized SBA-15. First, 6 g of Pluronic 123 (Aldrich 5800 average molecular weight) was dissolved in 200 g of 2 M sulfuric acid. Then 9.25 g of tetraethyl orthosilicate (TEOS, Fluka) was added under intense stirring and maintained at room temperature for 6 h, after which 5 g of gallium sulfate (Aldrich, 99%) and 12 g of zirconium sulfate (Aldrich, 98%) were added under intense stirring and maintained at room temperature for 2 h. Subsequently, the reactor was heated to 375 K and maintained at this temperature without agitation for 24 h, then cooled back to room temperature. An aqueous solution of ammonium hydroxide (20%) was added to obtain a neutral pH. The solution was then reheated to 373 K, maintained for another 24 h without agitation, and cooled back to room temperature. The final solid was filtered, washed with several portions of ammonium hydroxide, dried under nitrogen for 4 h, and extruded using the mother liquor as a binder (5 wt%). The 1×5 mm extrudates were calcinated in air at 573 K; these were designated solid A. The solid A was placed in a tubular reactor and treated in the presence of steam and an ammonium stream at 473 K for 3 h to cause some Ga and Zr migration out of the framework. This solid was then impregnated with an aqueous solution of Pt diamine-chloride compound (Aldrich, 98%) at room temperature and subsequently washed, filtered, and dried in air at 330 K for 3 h to produce solid B, with 0.3 wt% of Pt, and solid C, with 0.6 wt% of Pt. Then solids A, B, and C were calcinated in air at 573 K for 3 h, and at 673 K for another 3 h. Three final catalysts with different amounts of Pt—GaZr (A), Pt(0.3)GaZr (B), and Pt(0.6)GaZr (C)—were obtained. All were activated in H_2 spiked with 50 ppm of CS_2 at 473, 573, or 673 K for 2 h. A thermal treatment study to check surface structure stability was performed in nitrogen at 673 K for 2 days.

2.2. Catalyst characterization

The pore structure of the three catalysts was measured through nitrogen sorption experiments and BET or BJH analysis. The measurements were obtained using a Micromeritics ASAP 2010 apparatus at 70 K. Adsorption–desorption procedures were automatically performed with a 5-s equilibration time for each point. The software calculated the pore size distribution in the microporous region and the average pore radius in the mesoporous region. The concentrations of S, Zr, Ga, and Pt were determined by atomic absorption. The XRD, ^{27}GaNMR, and ^{29}SiNMR of findings in a similar catalyst were reported previously [12].

2.2.1. Acidity (IR)

Infrared (IR) spectroscopy of the catalysts was performed with a Perkin-Elmer FTIR with DGS using a specially designed cell and an ultra-thin film (0.1 mm) hung on a quartz spring (McBain thermobalance). The solids were dried in argon flow at 350 K for 2 h, and then in hydrogen flow at 400 K for 4 h, then degassed in a vacuum at 133 Pa for 20 min and analyzed by IR. The peaks in the regions 800–1000 cm^{-1} and 1100–1200 cm^{-1} were deconvoluted and the absorbencies compared. The vacuum-treated samples were contacted at room temperature with a stream of argon (5 cm^3/min) containing 0.1% pyridine. Then the cell was heated to 423 K and 473 K in argon to desorb the pyridine. The values of the weight loss and the IR signal were reported as μmol of pyridine per g of sample. Other samples of Ga/SBA-15, Zr/SBA-15, and Al/SBA-15 were analyzed using the same procedure.

2.2.2. Pt dispersion (CO adsorption)

The same IR cell was used to perform the CO (Linde, 99.99% purity) adsorption. The solids were dried in argon at 350 K and then contacted with flowing hydrogen for 1 h. The cell was finally evacuated to 13 Pa at room temperature before the IR measurements were started. The metallic function was characterized by stepwise adsorption of small doses of carbon monoxide at room temperature until saturation was achieved at 1330 Pa at 70, 100, 150, and 200 K (200 scans with a 2 cm^{-1} spectral resolution). The deconvoluted area of the peaks was calculated and used for relative comparisons.

2.2.3. X-ray photoelectron spectroscopy (XPS)

The spectra were obtained in a Bruker 300 apparatus (Mg cathode) with a power of 50 eV (ref. C_{1s}: 285.0 eV). XPS analysis was used to assess the metal dispersion on catalysts using peak area intensity (corrected) to measure atomic concentration. Binding energies were measured in fresh reduced catalysts. The Shirley-type background was subtracted, and the Zr, Ga, Si, and O species were measured by peak deconvolution and integration to obtain the area [13]. The signals are reported here as ratios of metal intensities to total metal intensities on the surface. At the low concentration used here, Pt was only feebly detected. Sensitivity factors of 5.56 (Pt4f), 4.22 (Ga2d), and 2.33 (Zr3d) were used for intensity calculations.

2.2.4. Chemical reactions

The effects of the operating variables were evaluated in a small-scale (fixed-bed pseudo-isothermal) radial-type microreactor with a volume of 30 cm^3, isothermally operated at different temperatures (450–490 K), residence times (0.2–1.0 h), and H_2/HC ratios (2–3) at a constant total pressure of 1.1 MPa. First, 10 g of catalyst pellets ground to a 0.1-mm particle diameter were introduced into the reactor and activated for 2 h at 473 K in the presence of hydrogen spiked with 50 ppm of CS_2. Light naphtha, or light naphtha plus 20% of 1-pentene, cyclopentane, or isopentane, was passed through the catalyst at the

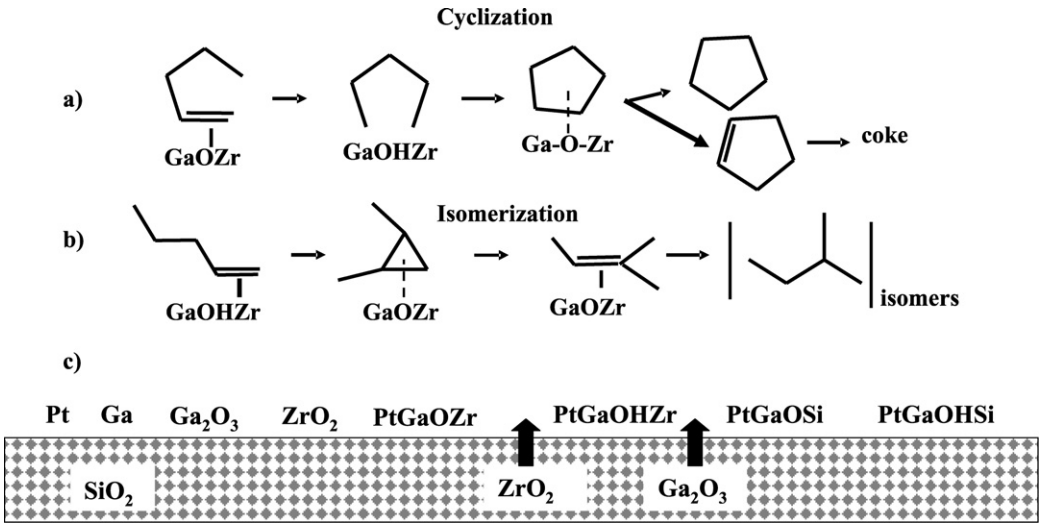

Fig. 1. Simplified paths of reactions: (a) cyclization, (b) isomerization, (c) surface components.

selected operating conditions for 1 h before the investigation of kinetic variables began. The products of the reaction were analyzed online using a Varian gas chromatograph equipped with a CP-Sil capillary column. The column activity was verified periodically using a standard sample, and reaction intermediates were tracked by mass spectrometry (Philips 2250). The conversion of pentane and hexane per mol under different operating conditions was calculated. (Selectivity is defined as mol of monoisomer formed to *n*-paraffin disappeared.) On the PtGaZr catalyst, the stationary state was achieved after 1 h, and the catalyst was stable for several days of operation.

For GaZr, activity declined as a function of time and temperature. A sequential procedure was used to determine the kinetics for three variables at three levels with the four feedstocks, as described earlier. Then, using a LH model for the in-series and parallel lump of reactions and a genetic algorithm previously developed by Bonilla [9], the data were processed to obtain the apparent kinetics constant with an error $<1\%$. The absence of mass and energy transfer control of the reaction was verified earlier using the experimental data [9]. The linear gas velocity (0.1 m/s) and the reactor radius (r_0: 10 mm, r_i: 2 mm) were selected based on the criteria developed by Bolton el al. [14], to avoid incorrect radial and axial gas flow distributions.

2.2.5. Path of reactions

The reaction paths for pentane and hexane proposed for this analysis and used in a lump model can be described as

$$n\text{-pentane} \underset{\text{GaZr+GaSi}}{\Leftrightarrow} \frac{\text{intemediary 1}}{\text{intemediary 2}} \underset{\text{GaZr+GaSi}}{\Leftrightarrow} \left\langle \frac{\text{cyclopentane}}{\text{isopentane} + \text{neopentane}} \right\rangle, \quad (1)$$

$$n\text{-hexane} \underset{\text{GaZr+GaSi}}{\Leftrightarrow} \frac{\text{intemediary 1}}{\text{intemediary 2}} \underset{\text{GaZr+GaSi}}{\Leftrightarrow} \left\langle \frac{\text{methylcyclopentane} + \text{cyclohexane}}{\text{isohexanes} + \text{di-isohexanes}} \right\rangle. \quad (2)$$

This model is based on two types of acid sites in which the heterogeneous reaction is controlled by surface isomerization steps, as discussed later in the paper. Simply stated, the paraffins adsorbed on Lewis and Brønsted (GaZr, GaSi) acid sites promote the formation of cyclo-intermediate 1, from which the cycloparaffin is formed, and intermediate 2, which leads to isoparaffin production. The metal provides the hydrides that regenerate the acid sites and control the polymerization. Fig. 1 shows a simplified picture of the reaction pathway.

2.2.6. Mass and energy balance for a radial reactor

The conversion of pentane and hexane as a function of residence time and temperature can be calculated based on mass, energy, and momentum equations developed for a centripetal plug-flow radial reactor (see Appendices A and B). The pioneer LH kinetics analysis for Pt/Al_2O_3 reported by Hosten and Froment [15] considered a heterogeneous model in which the surface isomerization stage is the rate-controlling step. We used the same approach here but included two sites, taking into account the preferential parallel adsorption of intermediates with no molecular hydrogen rate transfer control of the paraffin conversion.

3. Results

This section presents the results of the effect of Pt on the buildup of the two acid site active centers used for the conversion of C_5/C_6 into cycloparaffins and C_5/C_6 isomers. Fig. 1 depicts the surface reaction model (discussed in detail later in the paper). The model considers a Lewis site, used to adsorb the pentyl-cyclo structure to generate the cycloalkanes, and a Brønsted site, used to produce isomers through an intramolecular shift in various steps. On the surface, Pt, Ga, and Zr species may exhibit different degrees of reduction and interaction in generating acid sites (Fig. 1c). To elucidate the role of Pt, characterization of the catalyst surfaces is presented first, followed by discussions of catalyst activity, selectivity, and stability. Finally, the role of Pt in the path of reaction and on the acid sites is discussed.

3.1. Catalyst characterization

3.1.1. Catalyst structure

Table 1 shows that the three catalysts considered in this study had similar surface areas (roughly 180 m^2/g) and pore volumes (0.51 cm^3/g). Even when the method used during the initial part of the solid preparation was similar to that used for SBA-15 [11], the hydrothermal treatment modified the characteristic of the solids, and the SBA-15 hysteresis during nitrogen adsorption–desorption disappeared. This solid had a small microporous volume (0.1 cm^3/g). Table 1 shows that the catalysts had a SiO_2/Ga_2O_3 ratio of 15 and a SiO_2/ZrO_2 ratio of 20 (wt) and contained 0, 0.3, or 0.6 wt% of Pt. The Pt content is within the ranges of other commercial reforming or isomerization catalysts. The XRD analyses of the three samples are comparable to those reported previously [12] for a similar catalyst but with different amounts of Ga and Zr and zeolite precursor structures. The diffractograms (not shown) exhibited no defined signals associated with the cubic or monoclinic ZrO_2 or Ga_2O_3 species and showed a small bell shape in the background at 23°, associated with increases in the SiO_2 unit cells by Zr and Ga intercalated species in the framework. The poorly defined signal at 1° can be attributed to SiO_2 (currently present in the SBA-15 structure) in the low-angle region. The ^{71}GaNMR spectra, similar to those shown previously [12], exhibited three peaks: one at 7 ppm attributed to octahedral Ga^{3+} in Ga_2O_3, another at 150 ppm due to tetrahedral Ga^{3+} in a siliceous and zirconia environment in and out of framework, and a third at 175 ppm, assigned to tetrahedral Ga^{3+} out of framework. ^{29}SiNMR of the GaZr showed one main (broad) band at −110 ppm [Q^4-$Si(OSi)_4$] and two others at 101 ppm [Q^3-$Si(OSi)_3OH$] and 92 ppm [Q^2-$Si(OSi)_2(OH)_2$]. These bands were quite insensitive to the hydrogen treatment and were slightly shifted and broadened by the presence of Pt. The signals provided no additional insight into the change in –OH on the surface (total amount, ∼5.5 mmol/g) due to changes in Ga and Zr dispersion. Measuring OH with HNMR on hydrogen-treated GaZr sample gave 50% less OH than was measured by IR in the calcinated sample, due to the attenuation of the signal by "metallic" Ga. This technique is useless for Pt samples.

The amounts of Ga and Zr on the surface, as well as at the interface, depend on the hydrothermal treatment [9], which promotes the migration of this species out of the framework. The cluster of Ga, GaSi, Zr, and GaZr oxides formed were stable (XPS, IR, TEM) up to 673 K in nitrogen treatment for 2 days. Similar stability was found for GaZr on ZSM-5 and Mordenite by Freeley et al. [16].

Table 1
Physical and chemical properties of the catalysts

Properties	GaZr	Pt(0.3)GaZr	Pt(0.6)GaZr
Surface (m^2/g)	196	189	178
Pt (wt%)	0	0.3	0.6
SiO_2/Ga_2O_3 (wt%)		15	
SiO_2/ZrO_2 (wt%)		20	
Pores diameter (nm)	12.1	12.0	11.0

3.1.2. Metals on the surface

The catalyst contained several species on the surface besides siliceous oxide. To determine the effect of Pt on these chemical species, the GaZr and PtGaZr catalyst surfaces were evaluated by XPS and CO adsorption. Table 2 shows the XPS binding energies (BEs) and ratios of the peak intensity for the Ga and Zr signals with respect to the intensity of Si plus the other metals on the surface.

The Si2p presents a broad signal at 103.0 eV that is similar in GaZr and PtGaZr samples but different than the narrow ones observed for Ga/SBA-15 and Zr/SBA-15 at similar BE (102.9 eV), due to the contribution of Ga–Si and Zr–Si interactions. The Ga3d spectrum (Fig. 2, left side) is complex because of the tail of O^{2-} contributions that can be taken into account by deconvolution. It indicates a high concentration of tetrahedric Ga^{3+} on the surface (21.9 eV), as well as some Ga^+ or Ga^0 (20.1 eV). The $Ga2p_{3/2}$ exhibited two bands at 1120 and 1118.5 eV, confirming the presence of Ga^{3+} and Ga^+. Note the high BE of $Ga2p_{3/2}$, which represents a lower Ga-positive charge on these samples compared with that of Ga/SBA-15, which is quite similar to those observed in GaAl/SBA-15. The broadening of the Ga^{3+} bands (1120 and 21.9 eV) in GaZr with respect to those observed in Ga/SBA-15 suggests a bridging of Ga to the Zr species. The greater the amount of Pt, the higher

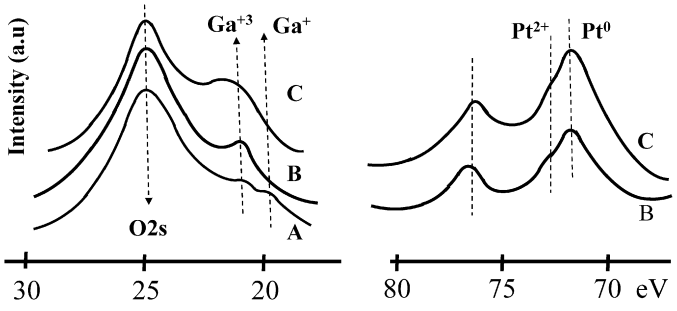

Fig. 2. Left side, XPS spectra of Ga in: (A) Pt(0.3)GaZr; (B) Pt(0.6)GaZr, (C) Pt(0.3)GaZr after reduction at 573 K in H_2. Right side, spectra of Pt in: (B) Pt(0.3) GaZr and (C) Pt(0.6)GaZr after reduction at 573 K.

Table 2
Ratio of Ga, Zr, or Pt signal intensity to total metals signals intensities (XPS) for GaZr, Pt(0.3)GaZr, and Pt(0.6)GaZr catalysts reduced at 473 K

Ratio of intensities	Metal (eV)					
	GaZr		Pt(0.3)GaZr		Pt(0.6)GaZr	
	$I_{Me}/I_{(TMe)}$	FWHM	$I_{Me}/I_{(TMe)}$	FWHM	$I_{Me}/I_{(TMe)}$	FWHM
$Ga3d_{5/2}$ (21.9)	1.5	1.85	1.3	1.9	1.45	2.1
$Zr3p_{5/2}$ (182, 9)	3.0	3.0	3.4	3.4	3.6	3.6
Pt4f (71.5; 72.4)	–	–	0.1	1.2	0.3	1.2

Table 3
Effect of hydrogen treatment temperature and chemical reactions on Ga^{+}/Ga^{3+} and Pt^{2+}/Pt^{0} ratios of XPS signals intensities for GaZr, Pt(0.3)GaZr, and Pt(0.6)GaZr catalysts

Catalyst	Ratio ($\times 10^2$) of intensities					
	Treated in H_2				After reaction (12 h)	
	At 473 K		At 573 K			
	Ga^{+}/Ga^{3+}	Pt^{2+}/Pt^{0}	Ga^{+}/Ga^{3+}	Pt^{2+}/Pt^{0}	Ga^{+}/Ga^{3+}	Pt^{2+}/Pt^{0}
GaZr	24.0	–	41.0	–	8.0	–
Pt(0.3)GaZr	38.0	12.0	72.0	10.0	55.0	24.0
Pt(0.6)GaZr	41.0	7.0	77.0	5.0	60.0	20.0

the dispersion and the reduction of Ga (Table 2); therefore, the Ga configuration on the surface is affected by Zr and Pt. Augmenting the pretreatment temperature to 573 K increased both the Ga reduction (Table 3, ratio Ga^{+}/Ga^{3+}) and dispersion for all catalysts. The effect of Pt content was similar to that observed at 473 K.

The $Zr3d_{3/2}$ and $Zr3d_{5/2}$ XPS peaks (182.9 and 185.3 eV, respectively) on the Pt(0.3)GaZr sample exhibited a 0.4-eV shift with respect to Zr/SBA-15 and a 0.3-eV shift with respect to GaZr sample, along with BEs similar to those observed in the SO_4Zr catalyst [17]. In addition, the dispersion of the Zr was increased (Table 2), and the size of the nanoclusters likely was reduced by the presence of Pt. Pt(0.6) demonstrated narrow Zr bands with no additional shift and a slightly higher dispersion. These effects also can be attributed to changes in the Ga species and the embedding of Pt [18]. In further reductions performed in hydrogen at 573 K, the bands narrowed and the dispersion increased; no additional shifts in the bands were observed, however. The effect of temperature is similar to that reported on Ga/silicalite by Shapiro et al. [19], who proposed an additional migration of Ga out of the framework by a reduction in hydrogen.

The XPS Pt ($Pt4f_{5/2}$ and $Pt4f_{3/2}$) signals for Pt(0.3) and Pt(0.6) catalysts reduced in H_2 at 473 K are shown in Fig. 2, left side. Under prolonged exposure to X-rays, the Pt was reduced, as was reported by Katrib [20]. For this reason, the spectrometer was set up for high pulse counting to reduce the effect of reduction and those of any retained anions (Cl^{-}, $SO_4^{=}$) at the expense of decreased resolution. The results show that the spectra after 20 min and those after 200 min were quite similar, demonstrating no reduction due to XPS beam energy. In both samples, spectra deconvolution can distinguish three species present on the surface: Pt^{2+} (73.0), $Pt^{\delta+}$ (72.4), and Pt^{0} (71.5 eV). The higher the amount of Pt, the stronger the signals of Pt^{0}, $Pt^{\delta+}$, and lower (slightly) the metals with no reduction. The small differences in Pt^{2+} species between the two catalysts suggest similar embedding on the surface clusters. Based on the ratio of intensities for Ga and Zr (Table 2), Pt can be clearly seen to play a role in the migration of these elements through its dispersion and stabilization on the surface. Diaz et al. [21] reported that increasing the Pt content, increased the extra-framework Ga species in the Ga/ZSM-5 system; they postulated that Pt is included in the Ga structure on the surface. The favorable effect of Pt on Zr dispersion on SZr also has been discussed in the literature [22–24].

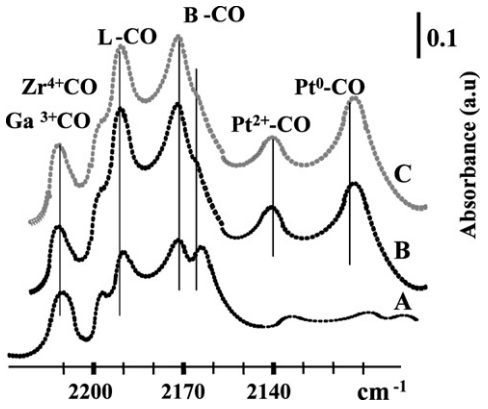

Fig. 3. Absorbance of CO (IR) on: (A) GaZr, (B) Pt(0.3)GaZr, (C) Pt(0.6)GaZr.

In our case, Pt^{0} was moderately dispersed on the surface, and $Pt^{\delta+}$ seemed to decorate the Ga–Si and GaZr species; however, information on Pt^{2+} is difficult to discern in a solid solution of tetragonally oriented Ga or octahedrally oriented Zr oxides. The greater the Pt content and the higher the H_2 treatment temperature used in the reduction, the greater the BE shift (from 72.8 to 73.1 eV) and the lower the Pt^{2+}/Pt^{0} ratio (Table 3). The ratio decreases are due to a higher dispersion of reducible Pt^{0} at quasi-constant $Pt^{\delta+}$ and lower Pt^{2+} content. Similar effects were reported on Pt/Al_2O_3 [24] and PtGa/ZSM-5 [25].

Finally, the bands of O1s exhibited a main peak (not shown) at 532.5 eV and two small peaks at 531.1 and 533 eV. The latter two peaks can be attributed to the coordination sphere of GaZr and GaSi clusters. This signal slightly augmented the presence of Pt, probably due to the greater dispersion of Ga and Zr on the surface. Treatment of the catalysts at 573 K produced a significant reduction of the O1s signal at 531 and 533 eV associated with the additional reduction of Ga and Zr, which destroys the Ga–Si and Ga–Zr interactions.

3.1.3. IR spectroscopy of adsorbed CO on Pt

IR spectroscopy of adsorbed carbon monoxide is often used as a fingerprint to measure the dispersion of platinum. Nevertheless, the low-temperature CO spectra was quite complex, with main (atop adsorption) bands at 2148 and 2139 cm^{-1} (ν(C–O): Pt^{2+}–CO), 2099 cm^{-1} (ν(C–O): Pt^{0}–CO); Fig. 3 shows the IR spectra recorded after adsorption at saturation (1330 Pa) at 70 K for the three catalysts. The three samples were dynamically degassed to verified peaks, and a complete desorption of CO was observed under vacuum (13 Pa) at 450 K. The

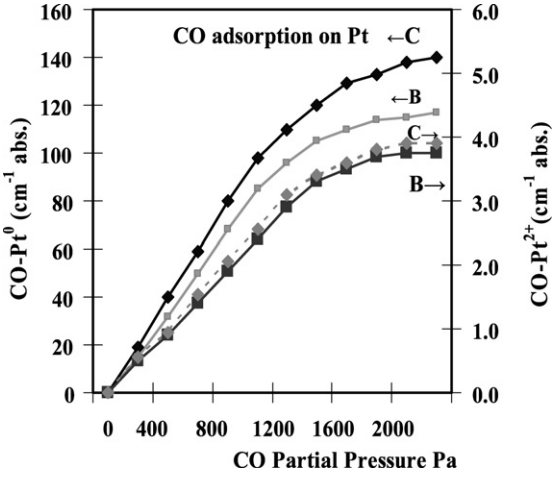

Fig. 4. Adsorption of CO on Pt^0 (left axis) and on Pt^{2+} (right axis) as a function of CO partial pressures for: (B) Pt(0.3)GaZr, and (C) Pt(0.6)GaZr catalysts.

important signals considered here in the Pt content catalysts were those of 2138 and 2091 cm^{-1}, which can be integrated using a FPI spectral deconvolution routine by adopting free and fixed parameters. Information about the strength of the adsorption was obtained by repeating the procedure at different incremental CO pressures ranging from 70 to 300 K on the two Pt-containing samples reduced at 473 K. The areas (cm^{-1} × abs.) calculated for the bands at 2138 and 2091 cm^{-1} were proportional to the CO adsorbed on Pt. Fig. 4 shows that at low coverage, linear CO adsorption occurred as a function of pressure, but then the interaction became weaker and the surface was saturated. The value at saturation (∼1200 Pa, 150 K) was used as a measure of dispersion. There was a small increment in the ratio of the amount of CO adsorbed on Pt^0 and Pt^{2+} [Eq. (3)] on Pt(0.6) with respect to that measured on the Pt(0.3) sample, due to the 2099 cm^{-1} band increase in a quasi-constant area of the 2139 cm^{-1} band. It is interesting to note that this ratio was slightly increased in both catalysts by the additional treatment of samples in hydrogen at 573 K for 8 h. This augmented the Pt dispersion and produced a small reduction in Pt^{2+}. The difference between the Pt(0.3) and Pt(0.6) was due mainly to the Pt^0 content. Note that the difference in CO adsorption at saturation (Fig. 3) was not proportional to the additional Pt content between samples B and C; thus, this additional Pt must have been located in larger Pt particles poorly dispersed on the SiO_2 surface. Eichler [26] also found the presence of a free and associated Pt cluster in a different environment oriented by zirconium oxide.

The saturation values measured at 200 K were half those measured at 150 K. This indicates the presence of different Pt species on the surface with different CO–Pt adsorption energies. Calculation of the total number of CO atoms adsorbed per atom of Pt content on Pt(0.3) at 150 K indicates an intermediate dispersion (65%) of the CO-accessible platinum. On Pt(0.6), only 45% of Pt accessibility could be obtained. The same calculation with the values measured at 200 K of adsorption temperature demonstrates that only 40% and 22% dispersion, respectively, was obtained for the two samples. The additional Pt content on Pt(0.6) seemed to go into clusters that grow with low CO–Pt adsorption energy:

$$\frac{[I_{2091}/I_{2138}]_{Pt(0.3)GaZr}}{[I_{2091}/I_{2138}]_{Pt(0.6)GaZr}} = 0.8\ (150\ K), \tag{3}$$

$$\frac{[I_{2091}]_{Pt(0.3)GaZr}}{[I_{2091}]_{Pt(0.6)GaZr}} = 0.73\ (150\ K), \tag{4}$$

and

$$\frac{[I_{2091}]_{Pt(0.3)GaZr}}{[I_{2091}]_{Pt(0.6)GaZr}} = 0.92\ (200\ K). \tag{5}$$

All of the previous information indicates that Pt on the surface was located mainly in small Pt clusters, moderately dispersed, and at the border (decoration) of GaSi and GaZr clusters. In addition, some Pt^{2+} was incorporated in later cluster structures.

3.1.4. IR spectroscopy of CO adsorption on acid sites

Fig. 3 shows the main bands for Brønsted (B) type of acid sites at 2165 and 2072 cm^{-1} (ν(O–H): Ga^{3+}–OH and Zr^{4+}–OH), and Lewis (L)-type bands at 2193 and 2210 cm^{-1}. The band at 2193 cm^{-1} was attributed by Mihaylov et al. [27] to the Zr^{4+}–CO observed in the $PtSZrCr/SiO_2$ catalyst; the band 2210 cm^{-1} may be due to Ga^{3+}–CO interactions. In addition, at low temperatures (70 K), a band attributed to physically adsorbed CO on Pt appeared at 2143 cm^{-1}. The bands attributed to the Brønsted- and Lewis-type sites were observed at 100 K but not at 300 K, indicative of the lower CO adsorption energy on acid sites than on Pt sites. The bands were deconvoluted, and the ratios of the L/B type [Eqs. (6) and (7)] were calculated at saturation conditions (700 Pa and 100 K for the two Pt-content catalysts). It can be seen that with higher amounts of Pt, the L/B ratio also increased. This may indicate a Pt-promoting effect of the Lewis acid by modification of Ga and Zr dispersion at the surface; nevertheless, the characterization of Lewis and Brønsted sites by this technique is quite difficult. But despite this difficulty, the relative values indicate that the total amount of acid sites decreased and the L/B ratio increased when the temperature of adsorption was augmented to 200 K, likely due to the desorption of CO from B and L sites with lower adsorption energies [see the values of Brønsted sites ratio for different amounts of Pt in Eqs. (8) and (9)]. At the same time, the bands at higher temperatures of adsorption narrowed and the CO absorbencies decreased:

$$\frac{[I_L/I_B]_{GaZr}}{[I_L/I_B]_{Pt(0.6)GaZr}} = 0.85\ (150\ K), \tag{6}$$

$$\frac{[I_L/I_B]_{Pt(0.3)GaZr}}{[I_L/I_B]_{Pt(0.6)GaZr}} = 0.92\ (150\ K), \tag{7}$$

$$\frac{[I_L]_{GaZr}}{[I_L]_{Pt(0.6)GaZr}} = 0.95\ (200\ K), \tag{8}$$

and

$$\frac{[I_L]_{Pt(0.3)GaZr}}{[I_L]_{Pt(0.6)GaZr}} = 0.90\ (200\ K). \tag{9}$$

3.1.5. IR spectroscopy of the catalysts

The FTIR spectra of the GaZr and PtGaZr catalysts before pyridine adsorption exhibited a broad band of symmetric

and asymmetric stretching at 400, 750, 800, 966, 1083, and 1086 cm^{-1}; a prominent shoulder a 1220 cm^{-1}; and those at 2200, 3248, 3614, 3685, 3755, and 3810 cm^{-1}. The 1083 and 1086 cm^{-1} frequencies correspond to Si–O–Si. It appears that the vibration was shifted toward higher wavenumbers, 6–9 cm^{-1} with respect to pure siliceous SBA-15 and Ga-Zr/SBA-15 and 12–14 cm^{-1} with respect to Zr/SBA-15. This confirms that the distortion of stretching was due to the interaction of Ga and Zr with silicon. The shoulder at 900 cm^{-1} and the bands at 1000 cm^{-1} (stretching of terminal sylanols) increased in intensity and were less well resolved than those on the Ga–Si or Zr–Si surface, likely due to the superimposed signal of the stretching of Si–O, Ga–O, and Zr–O. The 3614–3755 cm^{-1} region is attributed to –OH groups present in the Ga–Si and Ga–Zr environment out of the framework. The ratio of the intensities of these bands with respect to other bands increased slightly with the Pt content and with the temperature of the hydrogen treatment. Similar bands were found on PtGaAlZSM-5 [21]. The 400 cm^{-1} band corresponds to the rocking of Si–O–Si bridges. The band at 750 cm^{-1} is assigned to Zr–O vibrations [28], and the broad bands at 2200 cm^{-1} are assigned to the $Ga^{\delta+}$–H bond [29]. All of these findings suggest the partial incorporation of Ga and Zr into the siliceous surface structure already observed by XPS and ^{29}SiNMR.

3.1.6. IR spectroscopy of adsorbed pyridine

The surface of the catalyst contained various types of acid sites that may adsorb pyridine. Two of these were Brønsted types, one attributed to the –Ga–OH–Si– and the other to the –Ga–OH–Zr– hydroxyls on the surface. In addition, there were two possible Lewis sites with similar interactions as the previous ones (–Ga–O–Si– and –Ga–O–Zr–) but in different coordinating environments. Both Brønsted and Lewis acid sites can provide a broader distribution of acid strengths in accordance with the CO adsorption. IR analyses (not shown) of the adsorbed pyridine molecule detected the typical bands of pyridine at 1444, 1459, 1494, 1550, 1580, 1597, 1621, and 1640 cm^{-1} as reported in Ga–Si [30], along with those at 1448, 1470, and 1628 cm^{-1} attributed to ZrSi [31]. The 1620–1628 cm^{-1} and 1448–1456 cm^{-1} broad bands are attributed to coordinated pyridine in Ga–O–Si and Ga–O–Zr (Lewis acid sites), whereas those broad bands at 1545–1548 cm^{-1} are due to pyridinium coordinated to Brønsted acid sites. The catalyst also exhibited small bands at 1500 and 1680 cm^{-1} similar to those observed on Al-SBA-15, signaling a more complex pattern of adsorbed pyridine than on GaAl/ZSM-5 [32]. Table 4 gives the Brønsted (1544–1548 cm^{-1})/Lewis (1440–1460 cm^{-1}) ratios of the amount of pyridine that remained adsorbed at 300, 430, and 473 K, and the number of Lewis acid sites present on the samples reduced at 473 K. The higher the desorption temperature, the smaller and sharper the bands at 1546 and 1450 cm^{-1}, confirming the CO adsorption results indicating a greater contribution of fewer but stronger acid sites. Table 4 also shows that the greater the amount of Pt, the higher the total number of acid sites (B + L) and the greater the amount of pyridine that remained adsorbed on Lewis sites at 473 K. Thus, the Pt, which improves the Ga and Zr dispersions, developed a greater number of Lewis-type sites of greater strength.

Table 4
Ratio of pyridine adsorbed on Brønsted to pyridine adsorbed on Lewis acid sites at 300, 430 and 473 K; pyridine adsorbed on Lewis acid site (mmol/g) at 300, 430 and 473 K

Ratio B/L–Lewis (mmol/g)[a]	GaZr	Pt(0.3)GaZr	Pt(0.6)GaZr
B/L–Lewis (300 K)	1.9–1.12	2.1–1.23	2.2–1.33
B/L–Lewis (430 K)	0.22–0.38	0.28–0.4	0.25–0.5
B/L–Lewis (473 K)	0.10–0.18	0.14–0.2	0.12–0.3

[a] Brønsted/Lewis sites ratio–Lewis acid site.

Table 5
Normal pentane conversion and products distribution (mol%) for GaZr at 460 K, and for Pt(0.3)GaZr catalyst at 460, 470 and 480 K. Other operating conditions were: 2 H_2/HC ratio, 0.6 h residence time, and 1.2 MPa total pressure

	Feed	Catalyst			
		GaZr	PtGaZr(0.3)		
Temperature (K)		460	460	470	480
C_5 conversion (%)	0	27.90	33.56	44.34	54.42
Products (mol%)					
C_2–C_3	0	0.15	0.2	0.32	0.37
Butane	1.9	1.7	1.4	1.18	1.02
Methylpropane	2.91	4.08	4.38	4.6	4.76
Butene	1.07	0	0	0	0
n-Pentane	71.6	52.2	48.1	40.3	33
Pentene	0.8	0	0	0	0
Isopentane	1	10.2	12.6	18.4	23.1
Neopentane	0.1	4.7	5.5	6.4	7.3
Cyclopentane	0.4	6.8	7.7	8.8	10.5
n-Hexane	16.2	10.2	8.1	6.06	3.84
Hexene	0.34	0.00	0.00	0.00	0.00
Me-2 and 3-pentane	0.4	3.2	4.1	3	2
2,3-Methylbutane	0.88	1.93	2	2.55	2.7
2,2-Methylbutane	0.76	1.01	1.1	1.8	2.5
Ethyl-2-butane	0.7	0.52	0.9	1.4	2
Cyclohexane	0.7	1.47	1.99	2.7	3.85
Methyl-cyclopentane	0.05	1.2	1.15	1.56	2.1
Benzene	0.1	0.15	0.05	0.04	0.03
C_7 (total)	0.05	0.1	0.12	0.14	0.16
C_7 cycloparaffins	0	0.051	0.06	0.07	0.06
C_8 (total)	0.01	0.5	0.7	0.75	0.78
C_8 cycloparaffins	0	0.51	0.45	0.38	0.33

3.1.7. Effect of temperature and space velocity on activity and selectivity

The light naphtha used as the feedstock was composed mainly of *n*-pentane, as shown in Table 5. The table lists the main products of the reaction (start of run) for the GaZr catalyst at 460 K and for the Pt(0.3)GaZr catalyst at 460, 470, and 480 K.

The effect of temperature and residence time on C_5 and C_6 conversion are shown in Figs. 5 and 6, respectively, for Pt(0.3) and Pt(0.6) catalysts (data points) and GaZr (bars). The experimental points were obtained at three residence times and three temperatures for initial activity. The full line corresponds to the

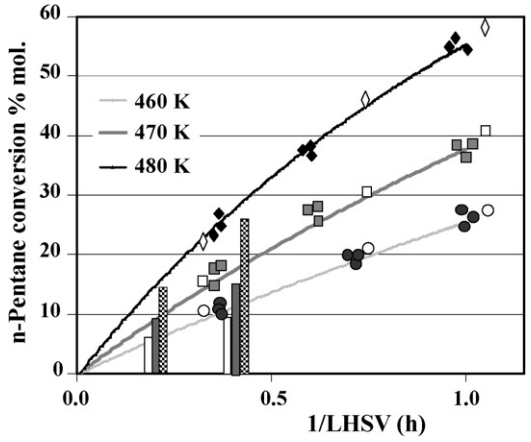

Fig. 5. Effect of temperature and residence time on normal pentane conversion (mol%); lines show the model prediction, black points ((●) 460, (▓) 470, (◆) 480 K) represent conversions for Pt(0.3)GaZr, and white points ((○) 460, (□) 470, (◇) 480) for Pt(0.6)GaZr; bars ((□) 460, (▓) 470 and (▒) 480 K) show conversions for GaZr catalyst.

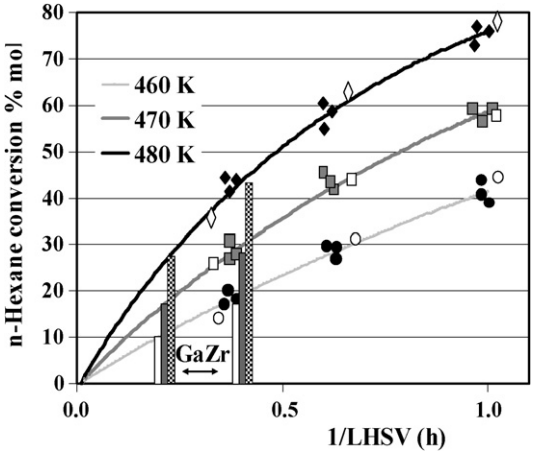

Fig. 6. Effect of temperature and residence time on normal hexane conversion (mol%); lines show the model prediction, black points ((●) 460, (▓) 470, (◆) 480 K) represent conversions for (Pt(0.3)GaZr, and white points ((○) 460, (□) 470, (◇) 480 K) for Pt(0.6)GaZr catalyst; bars ((□) 460, (▓) 470 and (▒) 480 K) show the conversions for GaZr catalyst.

model prediction using equations given in Appendix B. GaZr conversions >38% were impossible to measure because of the high deactivation of this catalyst during the first hour. The kinetics for this catalyst were explored using fresh catalyst for each trial. Conversion of *n*-paraffins into i-paraffins was augmented nonlinearly with space velocity and temperature. All of the conversions were similar in the presence of Pt(0.3) or Pt(0.6) (Fig. 4). The difference in activity between the latter two catalysts was not proportional to the Pt content. The ratios of activity ($\Delta F_{nP}/F_{nP0}$) obtained at 460 K and at 28% conversion using different space velocities show that the addition of 0.3% Pt increased the activity by 12%, but the addition of 0.6% PT increased activity by only 18% [Eqs. (10) and (11)]. Increasing the temperature to 470 K increased these ratios by 10% [Eq. (12)] and 12% [Eq. (13)], respectively. Clearly, most of the additional Pt added over the initial 0.3% was quite ineffective in the conversion, and the reaction became slightly less sensible to temperature:

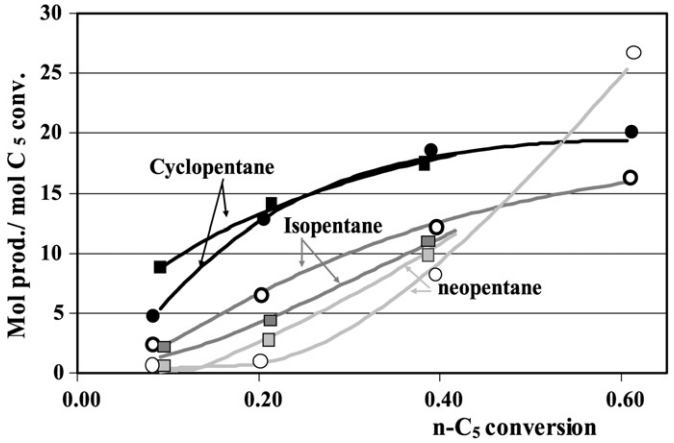

Fig. 7. Effect of Pt content on products formed from *n*-pentane (mol%); lines show the model predictions; square points ((■) cyclopentane, (▓) isopentane and (▒) neopentane) represent conversions for GaZr, and circle points ((●) cyclopentane, (O) isopentane and (○) neopentane) for Pt(0.3)GaZr catalyst.

$$\frac{[\Delta F_{nP}]^{C_5}_{Pt(0.3)GaZr}}{[\Delta F_{nP}]^{C_5}_{GaZr}} = 1.12\ (460\ \text{K}), \tag{10}$$

$$\frac{[\Delta F_{nP}]^{C_5}_{Pt(0.6)GaZr}}{[\Delta F_{nP}]^{C_5}_{GaZr}} = 1.18\ (460\ \text{K}), \tag{11}$$

$$\frac{[\Delta F_{nP}]^{C_5}_{Pt(0.3)GaZr}}{[\Delta F_{nP}]^{C_5}_{GaZr}} = 1.10\ (470\ \text{K}), \tag{12}$$

and

$$\frac{[\Delta F_{nP}]^{C_5}_{Pt(0.6)GaZr}}{[\Delta F_{nP}]^{C_5}_{GaZr}} = 1.12\ (470\ \text{K}). \tag{13}$$

3.1.8. Selectivity

The product distribution at 460 K was quite similar for both catalysts, despite the 20% higher paraffin content in the products of Pt(0.3). Both catalysts produced C_5 and C_6 cycloparaffins and a small amount of C_7 and C_8 hydrocarbons, whereas olefins, benzene, toluene, and xylene were mainly absent in the products at the temperatures and H_2/HC ratios used here. The hydrocracking reaction produced small amounts of C_2–C_3, which increased with temperature. Table 5 shows that neopentane (NP) and isopentane (iP) were formed far from their internal thermodynamic equilibrium ratios (e.g., the equilibrium for C_5 at 473 K was 14% neopentane, 16% *n*-pentane, and 73% molar isopentane plus cyclopentane). In any case, the isomerization steps toward di-isomers seemed to occur too slowly to form a large proportion of them. Table 5 shows that isobutane, isopentane, isohexane, cyclopentane, and methyl-cyclopentane were primary products and neopentane, 2,2- and 2,3-DMB were secondary products of the reactions. Different behaviors were observed for other isomerization catalysts, such as Pt–SZr [17].

The evolution of reaction products as a function of paraffin conversion for GaZr and Pt(0.3) and Pt(06) catalysts is shown in

Fig. 7. It can be seen that cycloparaffin production increased as a function of time, but the rate of production passed a maximum and then decreased slightly at higher conversions. Cycloparaffins and isoparaffins appeared to be intermediate products of the reaction, which were transformed into di-isomers. The induction period for di-isoparaffin formation is shown in Fig. 7. There the effect of Pt on selectivity can be seen, for example, by the ratio of cycloparaffin to isoparaffins at 20% C_5 conversion and two temperatures:

$$\frac{[N_{CP}/N_{iP}]^{C_5}_{Pt(0.3)GaZr}}{[N_{CP}/N_{P}]^{C_5}_{GaZr}} = 1.11\ (460\ K), \tag{14}$$

$$\frac{[N_{CP}/N_{iP}]^{C_5}_{Pt(0.3)GaZr}}{[N_{CP}/N_{iP}]^{C_5}_{GaZr}} = 1.05\ (480\ K), \tag{15}$$

$$\frac{[N_{CiP}/N_{iP}]^{C_5}_{Pt(0.6)GaZr}}{[N_{CP}/N_{iP}]^{C_5}_{GaZr}} = 1.17\ (460\ K), \tag{16}$$

and

$$\frac{[N_{CP}/N_{iP}]^{C_5}_{Pt(0.6)GaZr}}{[N_{CP}/N_{iP}]^{C_5}_{GaZr}} = 1.08\ (480\ K). \tag{17}$$

The ratio of moles of cycloparaffins (N_{CP}) to moles of isoparaffins (N_{iP}) is 11% higher with 0.3% of Pt compared to without Pt [Eq. (14)], but this ratio decreased slightly with increasing temperature [Eq. (15)]. After adding 0.6% Pt [Eqs. (16) and (17)], this same trend was observed, but only small benefits were seen in response to the extra Pt incorporated, indicating that these intermediaries were not directly affected by the metal itself. The ratio of neopentane (N_{NP}) to isopentane (N_{iP}) at two temperatures and at 0.20 of C_5 conversion for GaZr/Pt(0.6), and Pt(0.3)/Pt(0.6) are given by the following equations:

$$\frac{[N_{NP}/N_{iP}]^{C_5}_{Pt(0.3)GaZr}}{[N_{NP}/N_{iP}]^{C_5}_{Pt(0.6)GaZr}} = 0.88\ (460\ K) \tag{18}$$

and

$$\frac{[N_{NP}/N_{iP}]^{C_5}_{Pt(0.3)GaZ}}{[N_{NP}/N_{iP}]^{C_5}_{Pt(0.6)GaZr}} = 0.81(470\ K). \tag{19}$$

Equation (18) shows that the ratio of di-isomers to mono-isomers was reduced by 12% after addition of the extra 0.3% Pt to the catalyst. This effect was slightly greater at higher temperatures [compare Eqs. (29) and (28)] for the same level of C_5 conversion. In other words, the presence of Pt slightly improved the production of di-isomers to the detriment of mono-isomers.

3.1.9. Stability

Pt's main effect was on catalyst stability. Comparing the C_5 conversion measured after 12 h to that at the start of the reaction (1 h) yielded the following results (460 K, 0.4 h, 2 H_2/HC, 1.2 MPa):

$$\frac{[\Delta F_{nP}]^{C_5}_{12h}}{[\Delta F_{nP}]^{C_5}_{1h}} = 0.23(GaZr), \tag{20}$$

Table 6
Normal pentane conversion and products distribution (mol%) at 2 and 3 H_2/HC ratio for Pt(0.3)GaZr (460 and 480 K), and for Pt(0.6)GaZr catalyst (460 K). Other operating conditions were: 0.6 h residence time and 1.2 MPa total pressure

	Catalyst					
	Pt(0.3)GaZr				Pt(0.6)GaZr	
Temperature (K)	460		480		460	
H_2/HC (–)	2	3	2	3	2	3
C_5 conversion (%)	33.56	36	54.42	53.00	36.00	38.00
Products (mol%)						
C_2–C_3	0.20	0.25	0.37	0.44	0.26	0.44
Butane	1.40	1.37	1.02	0.95	1.40	1.30
Methylpropane	4.38	4.45	4.76	4.83	4.30	4.40
n-Pentane	48.10	46.23	33.00	34.00	45.70	43.50
Isopentane	14.60	15.65	25.10	23.40	16.20	17.20
Neopentane	6.50	6.30	8.30	8.50	6.40	6.30
Cyclopentane	4.70	5.00	7.50	7.70	4.80	4.90
n-Hexane	8.10	7.80	3.84	3.50	7.85	7.60
Isohexane	4.10	4.44	2.00	1.94	4.23	4.70
2,2-Methylbutane	2.00	1.94	2.70	3.80	2.00	1.90
2,3-Methylbutane	1.90	1.99	4.50	4.27	3.10	2.7
Cyclohexane	1.99	2.05	3.85	3.60	2.20	2.30
Methyl-cyclopropane	1.15	1.53	2.10	2.20	1.56	1.73

$$\frac{[\Delta F_{nP}]^{C_5}_{12h}}{[\Delta F_{nP}]^{C_5}_{1h}} = 0.935(Pt(0.3)GaZr), \tag{21}$$

and

$$\frac{[\Delta F_{nP}]^{C_5}_{12h}}{[\Delta F_{nP}]^{C_5}_{1h}} = 0.95(Pt(0.6)GaZr). \tag{22}$$

Adding Pt dramatically improved the catalyst stability, as reported previously for other isomerization catalysts as well. Chemical analysis of the carbonaceous deposit on the catalyst after 12 h was 6.5% (GaZr), 1.15% (Pt(0.3)), and 1% (Pt(0.6)) of carbon by weight of catalyst, in agreement with the residual activity of the catalyst. In addition, solid analysis by ^{13}CNMR indicated that the coke was more aromatic in the GaZr catalyst than in Pt(0.3) and Pt(0.6) catalysts (ratio of NMR bands at 145 ppm to that at 30 ppm). The effect of Pt is associated with the control of intermediaries 1 and 2 conversion into olefins and their subsequent polymerization by "activated" hydrogen.

3.1.10. Effect of H_2 partial pressure

To understand the role of Pt during the reaction, it is important to measure the effect of the partial pressure of hydrogen. In the present work, this was done by changing the H_2/HC ratio from 2 to 3 at a constant total pressure. Analysis of the activity and selectivity shows that small increases occurred in both at the temperatures studied. Table 6 presents the effect of hydrogen partial pressure for Pt(0.3) at 460 and 480 K and for Pt(0.6) at 460 K, at the same space velocity. At higher hydrogen partial pressure, the paraffin conversion and di/mono isoparaffin ratio increased slightly. At the same time, the amount of cyclo-intermediates increased, as did hydrogenolysis. In general, the distribution of isomers was quite similar for the two H_2 partial pressures used here. This result agrees with the information reported in the literature for the isomerization of butane [5,6].

The effect of Pt content and H_2 partial pressure on activity at the same temperature can be seen by comparing Eqs. (23) and (24) for 0.4 h, 460 K, and 1.2 MPa:

$$\frac{[\Delta F_{\mathrm{nP}}]^{\mathrm{C_5}}_{\mathrm{Pt(0.6)GaZr}}}{[\Delta F_{\mathrm{nP}}]^{\mathrm{C_5}}_{\mathrm{Pt(0.3)GaZr}}} = 1.08 \text{ (2 of } \mathrm{H_2/HC}) \tag{23}$$

and

$$\frac{[\Delta F_{\mathrm{nP}}]^{\mathrm{C_5}}_{\mathrm{Pt(0.6)GaZr}}}{[\Delta F_{\mathrm{nP}}]^{\mathrm{C_5}}_{\mathrm{Pt(0.3)GaZr}}} = 1.15 \text{ (3 of } \mathrm{H_2/HC}). \tag{24}$$

Note that when the hydrogen partial pressure was increased by 50% at constant total pressure, only a small (7%) increment in relative conversion occurred, whereas doubling the Pt content in the catalyst augmented the activity by only another 8%. The effect on selectivity can be analyzed using the following equations:

$$\frac{[N_{\mathrm{NP}}/N_{\mathrm{iP}}]^{\mathrm{C_5}}_{\mathrm{Pt(0.6)GaZr}}}{[N_{\mathrm{NP}}/N_{\mathrm{iP}}]^{\mathrm{C_5}}_{\mathrm{Pt(0.3)GaZr}}} = 1.05 \text{ (2 of } \mathrm{H_2/HC}) \tag{25}$$

and

$$\frac{[N_{\mathrm{NP}}/N_{\mathrm{iP}}]^{\mathrm{C_5}}_{\mathrm{Pt(0.6)GaZr}}}{[N_{\mathrm{NPi}}/N_{\mathrm{iP}}]^{\mathrm{C_5}}_{\mathrm{Pt(0.3)GaZr}}} = 1.12 \text{ (3 of } \mathrm{H_2/HC}). \tag{26}$$

These results confirm that increasing hydrogen partial pressure by 50% and doubling the Pt content produced only a 7% improvement in selectivity toward cycloparaffin production at a similar C_5 conversion rate (20%). The higher hydrogen partial pressure and the amount of Pt affected the hydrogen concentration on the surface but did not appreciably affect the reaction rate or selectivity and slightly improved catalyst stability (5%). On GaZr, the stability after 5 h on stream also was slightly improved by the hydrogen partial pressure, despite the absence of Pt, likely due to hydrogen spillover promoted by $Ga^{\delta+}$ or Ga^0. Nevertheless, GaZr catalyst stability remained seriously compromised for commercial applications.

3.1.11. Effect of adding 20% of 1-pentene to the feedstock

Some authors have speculated about Pt's role in producing an olefinic intermediary. To study the role of Pt in the presence of olefins, a blend of naphtha plus 20% 1-pentene was tested and compared with the light naphtha reported previously. The effect of residence time was studied for the Pt(0.3)GaZr catalyst (470 K, 2 of H_2/HC, and 0.19, 0.38, and 0.59 h of contact time); Fig. 8 shows the results. The presence of 1-butene slightly improved the initial conversion and selectivity to cycloparaffins. The most important result is that 1-butene disappeared rapidly and was not present in the product of the reaction even at low residence time. This may indicate the rapid conversion of 1-pentene into *n*-pentane that follows the reaction path outlined above. The plot shows that cycloparaffins are increased in small quantities, attain a maximum, and then decrease by hydrogenolysis to produce other isomers.

Next, Pt(0.6)GaZr was tested. The generation of products follows the same trend shown in Fig. 8. Pt's effect at two temperatures can be seen by comparing Eq. (28) with Eq. (27), and

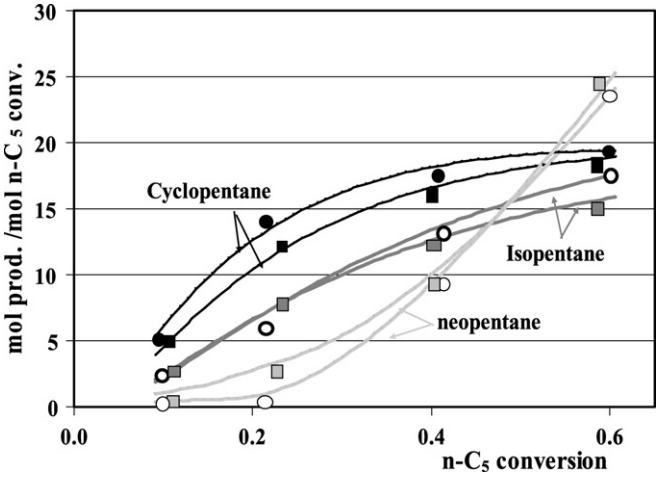

Fig. 8. Products distribution (mol%) from *n*-pentane isomerization as a function of residence time with and without 1-pentene in the feed (Pt(0.3)GaZr): (●) cyclopentane, (O) isopentane, and (○) neopentane for naphtha feed; (■) cyclopropane, (▓) isopentane and (▒) neopentane for naphtha plus 10% 1-pentene.

its effect on selectivity can be seen by comparing Eq. (30) with Eq. (29). Pt(0.6) showed a 7% higher C_5 conversion (460 K, 2 of H_2/HC, 0.4 h residence time) and 10% higher selectivity to cyclohexane compared with Pt(0.3), measured at around 40% *n*-C_5 conversion. These ratios changed with the conversion level used for the comparison, as shown by the shapes of the curves in Fig. 8. Any small change in performance generated by using Pt(0.6) instead of Pt(0.3) when 1-pentene was present in the feedstock cannot be attributed to additional hydrogenation capabilities, because the olefins disappeared very quickly and no additional intermediates were produced. Maurer and Kraushaar-Czarnetzki [33] investigated 1-pentene isomerization and found olefinic isomers on ZSM-5 but not on PtZSM-5, indicating low survival of these intermediates in the presence of hydrogen and Pt. Our earlier kinetic study of 1-pentene isomerization with a PtGa catalyst [9] found negligible olefin content and a high proportion of cyclopentane in the product. In the present study, no olefins were detected even at the highest temperature tested. The initial performance at different temperatures of the three catalysts can be fitted (±2%) by the model with similar activation energies, despite the differences in Pt content:

$$\frac{[\Delta F_{\mathrm{nP}}]^{\mathrm{C_5+1\text{-}but}}_{\mathrm{Pt(0.3)GaZr}}}{[\Delta F_{\mathrm{nP}}]^{\mathrm{C_5+1\text{-}but}}_{\mathrm{Pt(0.6)GaZr}}} = 0.93 \text{ (460 K)}, \tag{27}$$

$$\frac{[\Delta F_{\mathrm{nP}}]^{\mathrm{C_5+1\text{-}but}}_{\mathrm{Pt(0.3)GaZr}}}{[\Delta F_{\mathrm{nP}}]^{\mathrm{C_5+1\text{-}but}}_{\mathrm{Pt(0.6)GaZr}}} = 0.88 \text{ (470 K)}, \tag{28}$$

$$\frac{[N_{\mathrm{NP}}/N_{\mathrm{iP}}]^{\mathrm{C_5+1\text{-}but}}_{\mathrm{Pt(0.6)GaZr}}}{[N_{\mathrm{NP}}/N_{\mathrm{iP}}]^{\mathrm{C_5+1\text{-}but}}_{\mathrm{Pt(0.6)GaZr}}} = 0.90 \text{ (460 K)}, \tag{29}$$

and

$$\frac{[N_{\mathrm{NP}}/N_{\mathrm{iP}}]^{\mathrm{C_5+1\text{-}but}}_{\mathrm{Pt(0.3)GaZr}}}{[N_{\mathrm{NP}}/N_{\mathrm{iP}}]^{\mathrm{C_5+1\text{-}but}}_{\mathrm{Pt(0.60)GaZr}}} = 0.88 \text{ (470 K)}. \tag{30}$$

Table 7
Products distribution (mol%) with and without cyclopentane (CP) in the feed for GaZr, Pt(0.3)GaZr, and Pt(0.6)GaZr catalysts

	Catalyst					
	GaZr		Pt(0.3)GaZr		Pt(0.6)GaZr	
Feed[a]	Nap.	Nap. + CP	Nap.	Nap. + CP	Nap.	Nap. + CP
C_2–C_3	0.33	0.66	0.21	0.34	0.26	0.34
Butane	1.44	0.80	1.38	0.77	1.40	0.81
Methylpropane	4.22	4.11	4.38	3.98	4.30	4.11
n-Pentane	46.80	37.44	48.10	38.32	45.70	38.45
Isopentane	15.90	15.72	14.60	15.77	17.01	15.21
Neopentane	6.80	6.35	6.50	7.05	6.40	7.85
Cyclopentane	4.60	19.61	4.70	18.22	4.80	18.00
n-Hexane	7.90	5.30	8.10	5.42	7.85	5.50
Isopentane	4.30	3.81	4.10	3.91	4.23	4.05
2,3-Methylbutane	1.90	1.61	2.00	1.55	2.00	1.40
2,2-Methylbutane	2.00	1.70	2.00	1.70	2.20	1.73
Cyclohexane	1.88	1.44	1.99	1.59	2.20	1.63
Methyl-cyclopentane	1.26	1.00	1.15	0.91	1.56	1.11

[a] Naphtha or naphtha +10% of cyclopentane.

The test performed using the GaZr catalyst (460 K, $2H_2$/HC, 0.4 h residence time) demonstrated that when 1-butene was added to the naphtha, catalyst deactivation was too rapid, and after 2 h on stream, no conversion of paraffin occurred. At 470 K, it is impossible to measure the initial activity of GaZr at a residence time longer than 0.5 h, because of the accelerated deactivation of the solid. The products exhibited the presence of 0.5% benzene and hydrocarbons heavier than C_{10+}. These results indicate that the polymerization of olefin was fast and that the amount of active hydrogen on the surface was too low to control polymerization through hydrogenation.

The catalysts containing Pt(0.3) or Pt(0.6) lost 14% and 12%, respectively, of conversion after 12 h, demonstrating the favorable action of Pt in controlling the coke precursors.

3.1.12. Effect of adding 20% cyclopentane

Pt also may affect the production of cyclo-intermediaries. To gain insight into the effect of Pt on the formation of cyclo-intermediaries, 20% cyclopentane (CP) was added to the naphtha and tested with the three catalysts at around 36% nC_5 conversion (460 K, 2 of H_2/HC, and different space velocities). The results, reported in Table 7, indicate that an important reduction in nC_5 conversion occurred in the presence of cyclopentane plus naphtha, operating at the same degree of severity. To recover the same conversion with the new feed as obtained without CP in the feed, the residence time had to be increased by 34% for GaZr catalyst, 24% for Pt(0.3), and 21% for Pt(0.6).

The results indicate that at this level of C_5 conversion, approximately 20% of CP was converted into iso- and neopentane. Comparing the results with and without CP in naphtha show that the C_6/C_5 conversion ratio increased by around 10% with the presence of CP at constant nC_5 conversion. At equal nC_5 conversion (20%) with CP, the product distribution differed from that without CP in the feedstock. The presence of an initial amount of CP in the feed decreased the amount of cyclohexane, the di-isomer to mono-isomer ratio, and the (MCP + CH)/isohexane ratio in the product. These findings signal that the additional C_6 conversion (10%) was oriented to the production of iC_6 to the detriment of MCP, due to the competitive adsorption of CP on the same sites used by MCP intermediates. The strong adsorption of CP seems to be responsible for the reduced rate of nC_5 conversion. Using Pt(0.6) instead of Pt(0.3) did not appreciably alter the effect of CP on C_5 and C_6 selectivity, confirming the minor role of Pt in the kinetic rate of reactions and the major role of acid sites; additional hydrogenolysis was observed ($C_2 + C_3$), suggesting the influence of the metal content in this reaction. Similar effects were obtained by adding methyl-cyclopentane to the feedstock.

Considering catalyst stability, the GaZr catalyst lost 23% of its activity after 5 h on stream and was completely deactivated after 12 h, whereas in Pt(0.3) and Pt(0.6), the reduction was only 3% and 6%, respectively, after 12 h. The carbon content at the end was 6.33% (wt) in a spent GaZr. This coke content was slightly higher and more aromatic (^{13}CNMR analysis) than those measured (5.99%) without CP in the feed. Pt(0.3) and Pt(0.6) exhibited a somewhat similar amount of coke (1.84 wt%) after 12 h that was relatively less aromatic than the coke in GaZr. These observations support the idea that Pt preserves the catalysts and that coke precursors are formed from cyclo-intermediaries (Fig. 1a).

3.1.13. Effect of adding 20% isopentane

To study the effect of Pt on desorption of the isomer, 20% isopentane was added to the naphtha and the results compared with those obtained using pure naphtha. The results at 460 K, $2H_2$/HC, and 40% of C_5 conversion with the Pt(0.3)GaZr catalyst demonstrate that CP and MCP formation was unaffected by the isopentane. But this addition resulted in early production of neopentane and C_6 di-isomers, which increased by around 14%. Pt (0.6) and Pt (0.3) exhibited similar activity, selectivity, and stability with and without isopentane.

4. Discussion

4.1. Reaction mechanisms

It is noteworthy that the present catalysts work at temperatures 50–70 K lower than any other zeolite and SZr-type catalyst, but that the temperature is similar to that used for Pt/H-mordenite in commercial applications. At this low temperature, the C_5 isomerization equilibrium did not affect the conversion in the range of 20–60% used here. Very slight hydrogenolysis to C_2 and C_3 occurred due to pretreatment of the catalyst with sulfur.

The products observed in the present catalytic system of the reaction indicated a complex path of reactions occurring using two acid sites. In these sites, the intermediate 1 generates cycloparaffins, and the other intermediate leads to iso-C_5 and iso-C_6, which increase from the start of paraffin conversion (Fig. 8). Then they are converted into di-isomers after an induction period

The mechanism of isomerization and the role of metal and acid sites on bifunctional zeolite remain unclear. Two mechanisms for the isomerization of *n*-paraffins on FMI-type zeolites

have been proposed: monomolecular isomerization ([34–36] among others) with intramolecular rearrangement and bimolecular with intermolecular rearrangement ([37–39] among others). Risch and Wolf [40] reported that pentane and hexane follow a monomolecular path of reaction and mentioned the presence of two active sites that affect the initial activity and current activity; over a bifunctional catalyst (Pt/zeolite), the metal participates in dehydrogenation and the acid sites participate in isomerization of the olefins. However, Ono [41] reviewed these mechanisms and pointed out that isomerization is not so simple, because increasing the amount of Pt in mordenite produced no significant changes in selectivity, although improved stability was observed. Miyaji et al. [42] proposed that monomolecular and bimolecular mechanisms are present in several CsPWZr, SZr, and WZr catalysts for butane isomerization and characterized the roles of Pt and H_2 in controlling olefinic intermediates.

The roles of Brønsted and Lewis acid sites are also topics of discussion. Both types of sites reportedly are involved in activity and selectivity. Xiu and Sachtler [43] considered only Brønsted sites to be required for high activity and selectivity, but Pinna et al. [44] reported that the Lewis sites are important as well.

The catalyst used in the present work contains several species on the surface, as shown in Fig. 1c. The characterization found significant concentrations of Ga and Zr on the surface, due to their effective migration from the framework to the surface. Ga and Zr interact on the surface to form a cluster of GaZr and GaSi that generates 20% greater strong B acid and 35% greater L acid content (pyridine at 430 K) compared with those observed on Ga or Zr catalysts prepared on the same support by a similar procedure. The PtGaZr catalyst appears to be quite different than previous isomerization catalysts in terms of surface composition and selectivity. It demonstrated a lower but broader strength in total acidity and contained an intermediate B/L ratio compared with Pt/mordenite and SZr catalysts. PtGa is known to produce aromatics from propane and butane through bimolecular oligomerization and cracking. We demonstrated that for PtGaZr [9,10] prepared in other ways, a blend of cycloparaffins and aromatics was produced from ethylene and propylene with a bimolecular mechanism that goes through a cycloparaffin intermediate. The finding that cycloparaffin from pentane and 1-pentene was produced at more or less the same rate with a similar type of product suggests that the controlling step is intermediary isomerization, not hydrogenation or dehydrogenation. Kazansky [45] pioneered the concept of the formation of cyclo-intermediates using the –O and –OH groups on the surface. The GaZr and PtGaZr catalysts have these kinds of groups in the Ga–Si and Ga–Zr clusters in different proportions and with different structures. Pentane (and the hydrogenated 1-pentene) can be adsorbed by sharing a proton with a Lewis acid or from a Brønsted site. They are available with different strengths that can produce different adsorbed "activated" intermediates. These intermediates, at their lowest energy levels, reorganized to produce the final products. Pentane and hexane produced seemingly similar product distributions because they shared the same type of sites. Moreover, adding CP

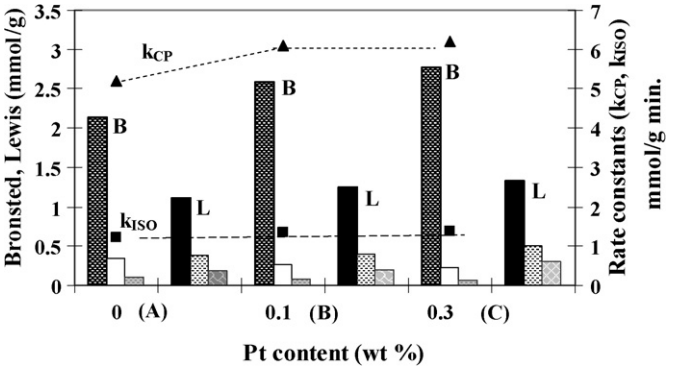

Fig. 9. Left axis, effect of Pt on the rate constant for pentane to cyclopentane (k_{CP}) reaction, and for pentane to isopentanes (k_{iso}) reaction (lines); right axis, effect of Pt on Brønsted ((▓) 300 K, (□) 430 K, (▒) 473 K) and Lewis ((■) 300 K, (▨) 430 K, (▩) 473 K) sites.

to the naphtha slightly increased the rates of isopentane and isohexane through diversion of the C_5 and C_6 conversion to the other sites unoccupied by CP. Therefore, there are two possibilities for reaction paths: (1) Cyclopentane is formed first in one site of the reaction, and then in series it is cracked to produce isopentane and the neopentane, or (2) cyclopentane and isopentane are formed in parallel in two different sites, and then cyclohexane is cracked into isopentane and neopentane.

To explain the effect of platinum, we selected the second option (fitted by the model with 10% lower deviation) because it better explains the foregoing results than the first hypothesis. Fig. 9 summarizes of the effects of Brønsted and Lewis sites using the reaction rate constants for cyclization (k_{CP}) and isomerization (k_{iso}). These constants were obtained using 54 experimental points for each catalyst and the equations given in Appendix B. Fig. 9 shows that the rate of cyclization increased in a nonlinear manner with increasing Pt content, in agreement with the Brønsted trend seen at low temperatures; notice that at high temperatures, the Brønsted trend was significantly decreased, whereas the Lewis trend improved. The isomerization rate constant did not vary with the Pt content. The results of Pd and CO analysis of the acid sites confirmed the presence of acid sites with different strengths. Because the reaction occurred at 460 K, only the strongest acids likely remained on the catalyst. In addition, at higher temperatures, the selectivity to cyclization also increased. Moreover, all of the spent PtGaZr catalysts exhibited a lower decrease in Lewis sites than in Brønsted sites (pyridine at 473 K), in agreement with lower cyclization deactivation compared with isomerization. Based on these findings, the cyclization can be attributed to the presence of Lewis sites, and the isomerization can be attributed to the Brønsted sites. At this point, we believe that intermediate 1, mentioned in Eq. (1), is an independent pentyl-cyclo-compound adsorbed in Ga–O–Zr and Ga–O–Si acid sites (Fig. 1a), whereas intermediary 2 [see Eq. (2)] is another cyclo-compound with different electronic and steric configurations (Fig. 1b) that is adsorbed on Ga–OH–Zr and Ga–OH–Si. The strength of acid sites seemed to be slightly modified by Pt decoration. This Pt also may have activated hydrogen and prevented the dehydrogenation of

this cyclo-structure into aromatic compounds or coke (Fig. 1a), thereby promoting acid site stability.

Our findings demonstrate that desorption of cyclo-alkanes from Lewis sites was limited by the CP partial pressure in the gas phase but desorption of isomers from Brønsted sites was not, but the latter may be limited by the partial pressure of isomers. In this way, depending on the type of cyclo-structure formed, the selectivity is oriented toward different products, and thus the acid site configuration seems to be critical to catalyst selectivity.

Note that using a large-pore silica material did not impede the formation of molecules larger than C_5 and C_6. Despite this, no hydrocarbons larger than C_8 were formed under the present operating conditions. Analysis of the small amount of C_{7-8} in the product of reaction confirmed the presence of dimethyl-cyclopentane, which might have been formed from butane dimerization (<4% wt in the feed) but not from pentane or hexane dimerization. The presence of C_2 and C_3 paraffins confirm some cracking activity. A bimolecular mechanism for C_5 and C_6 dimerization can be excluded.

The most thermodynamically favorable structure for these cyclo-structures was the C_5 cycle, which exhibited lower enthalpy formation than seen in the C_3, C_4, and C_6 cycles [46]. The reaction is supposed to occur as in reforming catalyst cyclization [47]. The absence of benzene and olefins in the product, as well the low survival of added 1-pentene, initially signaled the presence of an important "active" hydrogen concentration on the surface that can hydrogenate any olefin cycle-intermediates that are formed. We believe that complete delocalization of the electron to lose molecular hydrogen and form an olefin intermediate does not really occur in the presence of Pt and hydrogen. The intermediates of the reaction may be formed by sharing the proton to the L or from the B sites on a GaZr cluster structure, with no desorption of olefin compounds. The Lewis and Brønsted sites, which are useful for intermediate formation, must be of adequate strength and proper steric configuration to facilitate the adsorption and desorption that cannot be measured by pyridine atop adsorption. For this, the changes in activity do not correlate with the number of B or L sites, but follow the same trend.

Pt^{2+} (not reducible but accessible in the sublayer structure of the cluster) seems to play a role in the stabilization or promotion of the interaction of Ga and Zr that migrate toward the Si surface. This fraction of the platinum embedded in the subsurface of the gallium and zirconium, visible on XPS, modifies the electronic state of the Ga^{3+} and Zr^{4+} sites on the surface of the cluster and contributes in part to building different strengths on the acid sites. Nevertheless, the concentration of these sites was reduced by 55% after the reactions (Table 3; XPS results), whereas the activity loss was only 5%. Thus, the role of this Pt^{2+} remains unclear. Pt^0 and $Pt^{\delta+}$ at the border of the cluster provide the "active" hydrogen (spillover) to the acid sites and "isolate" intermediates 1 and 2 from the other neighboring intermediates, limiting their polymerization through hydrogenation. The findings that in the absence of Pt, some benzene appeared in the products and that a large amount of coke with high aromaticity was formed on the surface (^{13}CNMR analysis) confirm the aforementioned role of Pt. Some of these benefits of having Pt on the surface are lost by reduction of the sample in hydrogen at high temperature (673 K), as demonstrated by a 30% loss of activity and a 20% decrease in the cyclopentane/isopentane ratio. This treatment resulted in the disappearance of 25% of the Pt^{2+} species and reduced the total acidity by 35% and the B/L ratio by 35%. It seems that the additional Pt present on Pt(0.6) did not also promote isomerization activity by supplying more active surface acid sites and Pt^{2+} species with respect to the 0.3% Pt catalyst. The Pt in the latter catalyst already had occupied the potential position in the GaZr sites, and any excess went into Pt clusters.

Hydrogenation of olefins was rapid on the Pt sites, and the access of hydrogen to acid sites was sufficiently fast to limit the production of all olefins, particularly the well-known coke precursors cyclopentene and cyclopentadiene. Nevertheless, the additional amount of Pt, which may not be located at the border of GaZrSi clusters, did not significantly improve stability. The presence of sulfur on this intermediate dispersed cluster limited their hydrogenolysis.

5. Conclusion

This paper reports the effect of platinum content on the $PtGaZr/SiO_2$ catalyst used for the isomerization of light naphtha (mainly C_5) obtained from a refinery. The analysis of the product of the reaction indicates that the reaction might proceed without Pt with slightly lower activity and similar (but not identical) product distribution as those observed in the presence of Pt. The increased activity is due to the promotion by Pt of the migration of Ga and Zr to build and stabilize additional acid sites on the surface, even when the change in activity is not proportional to the change in acidity measured by pyridine adsorption. Lewis acid and Brønsted acid sites of the PtGaZr catalyst are stronger than those of Ga, Zr, and Al on the same support; however, the main role of Pt at the border of the Ga–O–Zr clusters is to substantially increase the catalyst stability. This Pt does not seem to affect the mechanism of reaction. The role of Pt^{2+} in the subsurface of the GaZr oxide clusters, although presently unclear, also may include electronic and steric promotion of some acid sites, resulting in slightly higher activity and selectivity. Based on kinetic analysis results, we can postulate that two different cyclo-intermediates of reaction are adsorbed on the surface at Lewis and Brønsted sites that orient the reaction toward different products. Pt in excess of 0.3% on the catalyst does not produce additional effects other than a slight modification of acidity. The stability of the active phase depends on the temperature of the reduction.

Acknowledgments

The authors thank I. Ramishaw for providing some of the IR measurements, R. Ravelo for constructing the radial reactor, P. Grange for engaging in valuable discussions, and Simon Bolivar University for providing financial support.

Appendix A. Nomenclature

Cp	gas heat capacity (J/(kg K))
d_p, d_h	particle and hydraulic diameter (m, m)
k_i	kinetics constant (mol/(L h))
MW	gas av. molecular weight (g/gmol)
P	pressure (MPa)
r, r_0	radius, reactor radius (M)
T	temperature (K)
x_i	conversion $(F_{io} - F_i)/F_{io}$ (–)
Y_i, Y_t	mole fraction i, total (–)
$\Delta P/L$	delta of pressure (Pa/m)

Greek symbols

γ_i	reaction rate (mol/(kg h))
ε_b	local bed voidage (–)
η	particle efficiency unit (–)
μ	viscosity (kg/(m s))
ρ	density (kg/m^3)
ϕ	Thiele module (–)

Appendix B. Equations used to solve the kinetics rate model

B.1. Mass balance for a radial reactor

$$\frac{dY_i}{dr} = -\frac{r}{r_0}\frac{\mathrm{MW}}{G_0}.V_r\eta_i\gamma_i, \tag{31}$$

where

$$V = \pi\cdot\left[r_0^2 - (r_0 - r)^2\right]L4; \quad V_r = V(1-\varepsilon_l). \tag{32}$$

B.2. Energy balance

$$\frac{dT}{dr} = -\frac{r}{G_0\cdot r_0\cdot \mathrm{Cp}_0}\left[\sum(-\Delta H_i)\cdot V_r\gamma_i\right]. \tag{33}$$

B.3. Momentum balance

$$\Delta P\frac{d_h}{L}\frac{2\rho_L}{G_L^2} = \frac{133}{\mathrm{Re}_L} + 2.33\left(\frac{0.4}{\varepsilon_l}\right)^{0.78}, \tag{34}$$

where

$$G_L = \frac{G}{(\varepsilon_l)} \tag{35}$$

and

$$d_h = \frac{4\varepsilon_b}{(1-\varepsilon_b)(6/d_p)}. \tag{36}$$

The voidage in the radial flow was determined experimentally and corresponds to the values reported by Bolton et al. [14]. The reactor performed in quasi-isothermal mode and with <1 °C difference in the radial and axial temperature profiles.

The rate constant for pentane disappearance can be written as follows for a surface chemical reaction with a controlling step on two acid sites:

$$\gamma_{nP5} = -\frac{dY_{nP5}/Y_t}{dt} = \frac{k_{5CP}(Y_{nP5} - Y_{CP}/K_{CP})}{[A + K_{CP}Y_{Cp} + K_{MCP}Y_{Cp}]} + \frac{k'_5(Y_{nP5} - Y_{iP5}/K_{iP5})}{[B + K_{iP5}Y_{iP5} + K_{iP6}Y_{iP6}]}. \tag{37a}$$

That for hexane can be written as

$$\gamma_{nP6} = -\frac{dY_{nP6}/Y_t}{dt} = \frac{k_{6CP}(Y_{nP6} - Y_{MCP}/K_{MCP})}{[A + K_{CP}Y_{CP} + K_{MCP}Y_{MCP}]} + \frac{k'_5(Y_{nP6} - Y_{iP6}/K_{iP6})}{[B + K_{iP5}Y_{iP5} + K_{nP6}Y_{nP6}]}. \tag{37b}$$

In the same way, the rate of iC_5 production is a function of both the rate of formation from nC_5 and CP and the rate of disappearance into neopentane. The boundary conditions for these equations are

$$r_0, \text{ any } L\text{: } Y_i = Y_0, \quad T = T_0, \quad P = P_0;$$
$$\text{and for } r = r, \quad Y_i = Y_i, \quad T = T_r \quad \text{and} \quad P = P_r. \tag{38}$$

In practice, step 1 (adsorption of paraffins) and step 3 (desorption of products) in the LH-type mechanism are considered at equilibrium. Intermediates 1 and 2 (cyclo-compounds) are formed in different acid sites and lead to different final products. As the reaction progresses, the cyclopentane and methylcyclopentane are slightly cracked into some isomers,

$$\gamma_{CP} = \frac{dY_{CP}/Y_t}{dt} = \frac{k_{5CP}(Y_{nP5} - Y_{CP}/K_{CP})}{[A + K_{CP}Y_{CP} + K_{MCP}Y_{MCP}]} - k'_{5Hyd}Y_{CP} \tag{39}$$

and

$$\gamma_{MCP} = \frac{dY_{MCP}/Y_t}{dt} = \frac{k_{6MCP}(Y_{nP6} - Y_{MCP}/K_{MCP}) - k_{6CH}Y_{MCP}}{[A + K_{CP}Y_{CP} + K_{MCP}Y_{MCP}]} - k'_{6Hyd}Y_{MCP}. \tag{40}$$

The efficiency is

$$\eta_i = \frac{3}{\phi}\left[\frac{1}{th\phi} - \frac{1}{\phi i}\right], \tag{41}$$

and the Thiele module is

$$\phi_i = \frac{3}{r_p}\sqrt{\frac{\gamma_i}{D_{eff}.C_i}}. \tag{42}$$

B.4. Numerical method

The set of differential equations were solved using a fourth-order Runge Kutta–Gil method programmed in Visual Basic 6. The conversions for the reactants were calculated from the experimental data obtained at different operating conditions. The genetic algorithm was seeded with the k_i and E_i values for the C_5 and C_6 reactions considered here. The convergence criteria compare the experimental value with the predicted one, and use

the difference to generate other k_i–E_i set of values or to finish the iterations,

$$\left[x^{\text{calc.}}_{\text{i-pentane}} - x^{\text{measured}}_{\text{i-pentane}}\right] < 2\%. \tag{43}$$

The rate of reaction constants was calculated using 54 experimental data points. The model is used to show the evolution of the species as a function of residence time, temperature, or conversion.

References

[1] X. Song, A. Sayari, Catal. Rev.-Sci. Eng. 38 (3) (1996) 329.
[2] F.R. Chen, G. Coudurier, J.F. Joly, J.C. Vedrine, J. Catal. 143 (1993) 616.
[3] S.R. Vaudagna, R.A. Comelli, S.A. Canavese, N.S. Figoli, J. Catal. 169 (2002) 389.
[4] H. Liu, G.D. Lei, W.M. Sachtler, Appl. Catal. A Gen. 137 (1996) 167.
[5] K. Watanabe, T. Kawakami, K. Baba, N. Oshio, T. Kimura, Catal. Survey Asia 9 (1) (2005) 17.
[6] G. Gianneto, G. Leon, J. Papa, R. Monque, R. Galiasso Tailleur, T.Z. Gabelita, Catal. Today 31 (1996) 317.
[7] T. Inui, A. Matsuoka, Prep. Pap. Am. Chem. Soc. Div. Pet. Chem. 36 (4) (1991) 670.
[8] L. Melo, P. Magnoux, G. Gianneto, F. Alvarez, M. Guisnet, J. Mol. Catal. A Chem. 124 (1997) 155.
[9] J. Bonilla, Isomerizacion de 1-penteno con catalizadores PtGaZr/SiO_2 y GaZr/SiO_2, Thesis, Simon Bolivar University (2001).
[10] R. Galiasso Tailleur, J. Bonilla Platin, Catal. Today 106 (2005) 77.
[11] S. Wu, Y. Han, Y.C. Song, L. Zhao, Y. Di, S.Z. Liu, F.S. Xiao, Chem. Mater. 16 (2004) 9739.
[12] R. Galiasso Tailleur, J. Bonilla Platin, Catal. Today 130 (2008) 527.
[13] D. Briggs, M.P. Seah (Eds.), Practical Surface Analysis by Auger and X-Ray Spectroscopy, Wiley, New York, 1987, p. 511.
[14] G.T. Bolton, C.W. Hooper, R. Mann, R.H. Stitt, Chem. Eng. Sci. 59 (2004) 1989.
[15] L.H. Hosten, G.F. Froment, Ind. Eng. Chem. Proc. Des. Dev. 10 (2) (1971) 280.
[16] J. Feeley, M. Deeba, R. Farrauto, G. Beri, A. Haynes, Appl. Catal. B Environ. 6 (1995) 79.
[17] D. Fuentes-Perujo, J. Santamaria-Gonzalez, J. Merida-Robles, E. Rodriguez-Castellon, A. Jiménez-Lopez, P. Maireless-Torres, R. Moreno-Tost, R. Mariscal, J. Solid State Chem. 179 (2006) 2182.
[18] J.M. Manoli, C. Potvin, M. Muhler, U. Wild, G. Resofszki, T. Buchholz, Z. Paál, J. Catal. 178 (1998) 338.
[19] E.S. Shpiro, D.P. Shevchenko, O.P. Tkachenko, R.V. Dmitrev, Appl. Catal. A Gen. 107 (1994) 147.
[20] A. Katrib, J. Electron Spectrosc. Relat. Phenom. 18 (1980) 275.
[21] Y. Diaz, L. Melo, M. Mediavilla, A. Albornoz, J. Brito, J. Mol. Catal. A Chem. 227 (2005) 7.
[22] M. Hino, K. Arata, Appl. Catal. A Gen. 160 (1998) 151.
[23] X.S. Liu, J. Thomas, J. Chem. Soc. Chem. Commun. 12 (1985) 1544.
[24] J. van Gestel, T. Nghiem Vu, D. Guillaume, J.P. Gilson, J.C. Duchet, J. Catal. 2121 (2002) 173.
[25] J.C. Duchet, D. Guillaume, A. Monnier, C. Dujardin, J.P. Gilson, J. van Gestel, G. Szabo, P. Nascimento, J. Catal. 198 (2001) 328.
[26] A. Eichler, Phys. Rev. B 71 (2005) 125418.
[27] M. Mihaylov, K. Hadjiivanov, H. Knosinger, Phys. Chem. Chem. Phys. 8 (407) (2006) 407.
[28] E. Rodriguez-Castellon, A. Jimenez Lopez, P.M. Maireles-Torres, D.J. Jones, J. Roziere, M. Trombetta, G. Busca, M. Lenarda, L. Storaro, J. Solid State Chem. 175 (2003) 159.
[29] S. Collins, M. Baltanas, J.L. Garcia Fierro, A.L. Bonivardi, J. Catal. 211 (2002) 252.
[30] C. Otero Arean, M. Rodriguez Delgado, V. Montouillout, J.C. Lavalley, C. Fernandez, J.J. Cuart, P.J. Parra, Microporous Mesoporous Mater. 67 (2004) 259.
[31] S. Damyanova, L. Petrov, M.A. Centeno, P. Grange, Appl. Catal. A Gen. 224 (2002) 271.
[32] Z. Gabelica, C. Mayenez, R. Monque, R. Galiasso, G. Giannetto, Synth. Microporous Mater. 1 (1992) 190.
[33] T. Maurer, B. Kraushaar-Czarnetzki, J. Catal. 187 (1999) 202.
[34] M. Guisnet, P. Andy, Y. Boucheffa, N.S. Gnep, C. Travers, E. Benazzi, Catal. Lett. 50 (1998) 159.
[35] A. Chica, A. Corma, J. Catal. 187 (1999) 167.
[36] G.D. Svoboda, E. Vynckier, B. Debrandere, G.F. Froment, Ind. Eng. Chem. Res. 34 (11) (1995) 3793.
[37] J. Denayer, G.V. Baron, G. Vanbutsele, P.A. Jacobs, J.A. Martens, J. Catal. 190 (2000) 463.
[38] V.B. Kazansky, I.N. Senchenya, J. Catal. 119 (1989) 108.
[39] D. Rutenbeck, H. Papp, D. Freude, W. Schweiger, Appl. Catal. A Gen. 206 (2001) 57.
[40] M. Risch, E.E. Wolf, Catal. Today 62 (2000) 255.
[41] Y. Ono, Catal. Today 81 (2003) 3.
[42] A. Miyaji, T. Echizen, L. Li, T. Susuki, Y. Yoshinaga, T. Okuhara, Catal. Today 74 (2002) 291.
[43] B.Q. Xiu, W.M.H. Sachtler, J. Catal. 167 (1997) 231.
[44] F. Pinna, M. Signoretto, G. Strukul, G. Cerrato, C. Morterra, Catal. Lett. 26 (1994) 339.
[45] V.B. Kazansky, Acc. Chem. Res. 24 (1991) 379.
[46] J.W. Pan, D. Rogers, F. McLafethy, J. Mol. Stuct. (Theochem) 468 (1999) 59.
[47] H. Du, C. Fairbridge, H. Yange, Z. Ring, Appl. Catal. A Gen. 190 (2000) 469.